Research Article

NMR IN BIOMEDICINE

Received: 10 April 2008, Revised: 29 January 2009, Accepted: 2 February 2009, Published online in Wiley InterScience: 2009

(www.interscience.wiley.com) DOI:10.1002/nbm.1387

Assessment of ^{31}P-NMR analysis of phospholipid profiles for potential differential diagnosis of human cerebral tumors

Juan Solivera[a]*, Sebastián Cerdán[b], José María Pascual[c], Laura Barrios[d] and José María Roda[e]

We describe a novel protocol for the non-histological diagnosis of human brain tumors *in vitro* combining high-resolution ^{31}P magnetic resonance spectroscopy (^{31}P-MRS) of their phospholipid profile and statistical multivariate analysis. Chloroform/methanol extracts from 40 biopsies of human intracranial tumors obtained during neurosurgical procedures were prepared and analyzed by high-resolution ^{31}P-MRS. The samples were grouped in the following seven major classes: normal brain ($n = 3$), low-grade astrocytomas ($n = 4$), high-grade astrocytomas ($n = 7$), meningiomas ($n = 9$), schwannomas ($n = 3$), pituitary adenomas ($n = 4$), and metastatic tumors ($n = 4$). The phospholipid profile of every biopsy was determined by ^{31}P-NMR analysis of its chloroform/methanol extract and characterized by 19 variables including 10 individual phospholipid contributions and 9 phospholipid ratios. Most tumors depicted a decrease in phosphatidylethanolamine (PtdEtn) and phosphatidylserine (PtdSer), the former mainly in neuroepithelial neoplasms and the latter in metastases. An increase in phosphatidylcholine (PtdCho) and phosphatidylinositol (PtdIns) appeared predominantly in primary non-neuroepithelial tumors. Linear discriminant analysis (LDA) revealed the optimal combination of variables that could classify each biopsy between every pair of classes. The resultant discriminant functions were used to calculate the probability of correct classifications for each individual biopsy within the seven classes considered. Multilateral analysis classified correctly 100% of the normal brain samples, 89% of the meningiomas, 75% of the metastases, and 57% of the high-grade astrocytomas. The use of phospholipid profiles may complement appropriately previously proposed methods of intelligent diagnosis of human cerebral tumors. Copyright © 2009 John Wiley & Sons, Ltd.

Keywords: ^{31}P-MRS; human brain tumors; phospholipid profiles; linear discriminant analysis; intelligent diagnosis

INTRODUCTION

Magnetic resonance spectroscopy (MRS) offers a variety of procedures to assess the metabolic alterations that occur in cerebral neoplasms, helping to obtain diagnostic decisions in a manner complementary to that provided by classical histopathology. ^{1}H-MRS has been most widely used in this context, in combination with elaborate statistical approaches, to classify the histological type of the brain tumor and its grade of malignancy (1–6). These studies are mainly focused in the profile of water soluble metabolites *in vivo* or *ex vivo*, as detected by ^{1}H MRS or ^{1}H HRMAS (high-resolution magic angle spinning). However, the

* *Correspondence to: J. Solivera, Laboratory for Imaging and Spectroscopy by Magnetic Resonance (2.12), Instituto de Investigaciones Biomédicas 'Alberto Sols' CSIC/UAM, c/ Arturo Duperier 4, E-28029 Madrid, Spain. E-mail: juan.solivera@gmail.com*

a *J. Solivera*
Department of Neurosurgery, Hospital Universitario Reina Sofía, Córdoba, Spain

b *S. Cerdán*
Institute of Biomedical Research 'Alberto Sols', Consejo Superior de Investigaciones Científicas (CSIC), Madrid, Spain

c *J. M. Pascual*
Department of Neurosurgery, Hospital Universitario de la Princesa, Madrid, Spain

d *L. Barrios*
Computing Technical Center (CSIC), Madrid, Spain

e *J. M. Roda*
Department of Neurosurgery, Hospital Universitario La Paz, Madrid, Spain

Contract/grant sponsor: Spanish Ministry of Education and Science; contract/grant numbers: SAF 2004-03197 and NAN 2004-09125-C07-03.
Contract/grant sponsor: Community of Madrid to SC; contract/grant number: S-BIO/0179/2006.

Abbreviations used: *1-lysoPtdSer, 1-lysophosphatidylserine; alkyl-acyl-PtdCho, alkylacylphosphatidyl-choline; $CDCl_3$, deuterated chloroform; Cer, ceramide; Cer-1-P, ceramide-1-phosphate; Cho, choline; DAG, diacylglycerol; DPG, diphosphatidylglycerol (cardiolipin); Etn, ethanolamine; EtnPlas, ethanolamine plasmalogen; FFA, free fatty acids; GroPCho, glycerophosphocholine; GroPEtn, glycerophosphoethanolamine; LDA, linear discriminant analysis; LysoPtdCho, lysophosphatidylcholine; LysoPtdEtn, lysophosphatidylethanolamine; PA, phosphatidic acid; PCho, phosphocholine; PDE, phosphodiester; PEtn, phosphoethanolamine; PI3K, phosphatidylinositol 3-kinase; PKC, protein kinase C; PLC, phospholipase-C; PME, phosphomonoester; PtdCho, phosphatidylcholine (lecithin); PtdEtn, phosphatidylethanolamine (cephalin); PtdIns, phosphatidylinositol; PtdSer, phosphatidylserine; SM, sphingomyelin; Sph-1-P, sphingosine-1-phosphate; TEtn, sum of ethanolamine phospholipids phosphatidylethanolamine + ethanolamine plasmalogen; WHO, World Health Organization.*

alterations in phospholipid metabolism detected during neoplastic transformations may offer an additional source of information useful to improve the earlier methods and obtain a more precise diagnostic orientation (7,8). In the present study, we investigate the use of phospholipid profiles obtained from tumor biopsies as tools in the intelligent diagnosis of cerebral neoplasms.

It has been shown previously that the phospholipid composition of cell membranes is altered in human cerebral neoplasms, as investigated by *in vivo* and *in vitro* ^{31}P magnetic resonance spectroscopy (^{31}P-MRS) (9). Two resonances of *in vivo* ^{31}P-MRS, reveal the changes in phospholipid metabolism: the phosphomonoester (PME) and the phosphodiester (PDE) resonances (10). When aqueous extracts of a tissue are analyzed *in vitro* by high-resolution ^{31}P-MRS, the PME signal can be resolved in the phospholipid precursors, phosphocholine (PCho) and phosphoethanolamine (PEtn), whereas the PDE peak includes the degradation products glycerophosphocholine (GroPCho) and glycerophosphoethanolamine (GroPEtn) (11). The PME resonance has been found to be increased in tumors and proliferating tissues in general, a change mainly explained by an accumulation of PCho and PEtn. On these grounds, changes in PME have been suggested as indicators of tumor progression or response to therapy (7,12,13) and the ratios PCho/GroPCho and PEtn/PCho have been proposed as indicators of malignancy. These alterations may involve not only a stimulated phospholipid biosynthesis, but also an increased degradation of phosphatidylcholine (PtdCho) and phosphatidylethanolamine (PtdEtn) (7,14).

To our knowledge, few studies have investigated the phospholipid composition of brain tumors by means of *in vitro* ^{31}P-MRS of organic extracts from tissue biopsies (15–17). Unlike *in vivo* ^{31}P-MRS and *in vitro* ^{31}P-MRS of aqueous extracts, this method can detect and quantify individually the major membrane phospholipids. Previous ^{31}P-MRS studies on phospholipid profiles of human brain tumors *in vivo* or *in vitro* were predominantly descriptive, with limited diagnostic value for the assignment of histological tumor type or grade of malignancy. In this work, we report a pilot study on the use of linear discriminant analysis (LDA) to classify the phospholipid profiles of a healthy brain tissue and different human intracranial tumors, as obtained by *in vitro* high-resolution ^{31}P-MRS analysis of organic extracts of these tissues (5).

EXPERIMENTAL

Human tumor biopsies

All procedures followed the bioethical guidelines of the Clinical Research Committees of the University Hospital 'La Paz' and fulfill the requirements of the responsible governmental agency. Thirty-seven biopsies of representative intracranial tumors were obtained during surgical procedures: high-grade astrocytomas (World Heath Organization (WHO) grades III–IV, $n = 7$), low-grade astrocytomas (WHO grades I–II, $n = 4$), oligodendrogliomas ($n = 2$), ependymoma ($n = 1$), central neurocytoma ($n = 1$), choroid plexus papilloma ($n = 1$), gliosarcoma ($n = 1$), meningiomas ($n = 9$), schwannomas ($n = 3$), pituitary adenomas ($n = 4$), and metastatic tumors ($n = 4$). The solid part of the neoplasm was extracted from the brain without the use of bipolar coagulation and split into two nearly similar portions, one of them was used for ^{31}P-NMR spectroscopy and the other for pathological diagnosis following the WHO criteria (18). Necrotic, cystic, hemorrhagic, or previously coagulated areas of the lesion were avoided. The biopsy to be used in ^{31}P NMR spectroscopy was immediately frozen in liquid nitrogen and stored at -82°C until the processing time (5). Additionally, three samples of the normal brain could be obtained during epilepsy surgery or lobectomy for the removal of malignant gliomas. In these cases, the tissue was removed far from the lesion to avoid contamination, and it was further processed in an identical manner to that described for the tumor samples.

Phospholipid extraction and preparation for high-resolution ^{31}P-MRS analysis

The extraction of phospholipids from tumor biopsies was performed using the classical method described by Folch (19) with the modifications of Meneses (20) and Merchant (21). Each biopsy was carefully weighed, pulverized, and homogenized in a 10 weight–volume ratio (g/mL) of chloroform/methanol (2:1, v/v) in a solid CO_2/methanol bath (-70°C). Methanol was then added to the homogenate up to an additional 20% of the initial volume and centrifuged (15 min, 8500 rpm, 4°C). After centrifugation, the supernatant was poured into a decantation funnel and the 2:1 proportion of chloroform/methanol recovered through the addition of chloroform up to 40% of the initial homogenate volume. The extracts were washed with EDTA-K 0.2 M at pH 6.0 and left overnight at room temperature (20–25°C). Typically, two liquid phases were observed in the funnel: an aqueous upper phase and a lower organic phase. The organic chloroform-rich layer was recovered in a polypropylene tube and evaporated in a stream of nitrogen gas.

Dried extracts were resuspended in 0.5 mL of a chloroform/deuterated chloroform (1:1, v/v) solution and transferred into a 5 mm diameter magnetic resonance test tube. The extracts were then washed with 0.3 mL of a methanol/EDTA-Cs 0.2 M at pH 6.0 (2:1, v/v) solution. Two phases could be observed in the definitive sample: a small aqueous upper phase and a much larger organic lower phase which was used later for ^{31}P-MRS analysis. The final proportion in the ternary system chloroform/methanol/EDTA-Cs was 100/40/20 (22).

^{31}P-MRS

^{31}P-NMR spectroscopy was performed at 11.7 Tesla, using a Bruker DRX 500 spectrometer (Bruker Biospin, Rheinstetten, Germany) operating at 202.4 MHz for ^{31}P. Before analysis, samples were allowed to warm up to room temperature. The organic phase in the MRS tubes was centered on the radiofrequency transmitter coil. The temperature of the probe was set at 25°C. $CDCl_3$ (99% D) was used to provide the lock signal and prevent drifting of the magnetic field during the acquisition. Acquisition parameters were: pulse width 7 μs (60° spin-flip angle), sweep width 10 kHz, 6 s total cycle time, free induction decays (FIDs) of 32 K acquired during 1 s and approximately 1300 scans. Gated proton broad-band decoupling, switched off during the relaxation delay, minimized the nuclear overhauser enhancement (NOE) effect (23). The resulting ^{31}P-MRS spectra were processed with the latest available version of Bruker 1D WIN-NMR software (v. 6.1). The processing parameters were: zero filling of 64 K,

Fourier transformation with line broadening of 0.5 Hz and automatic phase correction with minor manual adjustments. The PtdCho resonance, at −0.84 ppm, was used as an internal reference. Integrals were then calculated by fitting Lorentzian curves to the corresponding peak. Values are finally reported in molar percentages (24), as obtained from these peak integrals:

$$\%M(f) = \frac{I_f}{m_f \cdot \sum_{i=1}^{n} I_i} \quad (1)$$

where $\%M(f)$ is the molar percentage of a given phospholipid f, I_f represents the integral of phospholipid f peak, m_f the number of ^{31}P nuclei in the phospholipid (two in diphosphatidylglycerol 'cardiolipin' and one in the rest of the identified phospholipids), n the total number of phospholipid resonances included in the analysis, and ΣI_i is the added integrals of the considered phospholipid resonances 1 to n.

The assignment of resonances was performed with the aid of chemical shift values reported in the literature (16,17,20,22,25) and confirmed when necessary by the addition of authentic standards. Ten phospholipids were routinely detected: phosphatidic acid (PA), diphosphatidylglycerol (DPG), ethanolamine plasmalogen (EtnPlas), PtdEtn, phosphatidylserine (PtdSer), sphingomyelin (SM), lysophosphatidylcholine (LysoPtdCho), phosphatidylinositol (PtdIns), alkylacylphosphatidylcholine (Alkyl-acyl-PtdCho), and phosphatidylcholine (PtdCho). In addition, the following phospholipid ratios were investigated: PtdEtn/PtdCho, TEtn/PtdCho (TEtn: sum of ethanolamine phospholipids PtdEtn + EtnPlas), PtdSer/PtdCho, PtdIns/PtdCho, PtdEtn/PtdSer, TEtn/PtdSer, PtdIns/PtdEtn, PtdIns/TEtn and PtdIns/PtdSer. Taken together, these variables reflect the main phospholipid metabolic pathways altered in neoplastic transformations (7,26).

Statistical analysis

Statistical analyses were performed with the SPSS (v 11.5, SPSS Inc., Chicago, IL, USA) and SAS (SAS Institute, Inc., Cary, NC) packages operating on a Windows XP platform. Only tumor classes with three or more samples were considered for statistical evaluation. A total of 34 samples were finally included in the analysis ($n = 34$). First, a univariate statistical analysis was performed using the student's t test to systematically compare the differences in the phospholipid profile between all possible pairs of tumor classes and identify the variables that better explain the differences between every pair of classes in the discriminant analysis. Mann Whitney's U tests were also performed, yielding results very similar to those from Student's t test. The significance threshold was set at $p < 0.05$.

Second, a multivariate step-wise LDA was carried out to determine the best combination of phospholipids or phospholipid ratios that could optimally discriminate between every pair of tissue classes (27,28). For this purpose, only the most relevant variables after student's t tests were used: EtnPlas, PtdEtn, PtdSer, SM, PtdIns, PtdCho as well as their corresponding ratios. Overall, these variables showed a normal (Gaussian) behavior in the normality plots and tests (Kolmogorov–Smirnov and Shapiro Wilk). Homoscedasticity was also verified by using boxplots and Levene's test. As described previously in more detail (5), Fisher discriminant functions were calculated for all possible pairs of classes (bilateral classifications), and the probabilities inferred from these equations were later used to classify every sample amongst the seven possible classes (multilateral classification). Briefly, for the classification of a biopsy between two different tumor classes, i and j, the Fisher functions f_i and f_j (eqns (2) and (3)) include the linear combination of phospholipid variables x_t that best discriminate between the pair of tissue classes compared (27).

$$f_i = \sum_{t=1}^{k} a_{it} x_t + a_0 \quad (2)$$

$$f_j = \sum_{t=1}^{k} b_{jt} x_t + b_0 \quad (3)$$

The classification functions contain independent terms a_0 and b_0 and each variable is multiplied by a coefficient a_{it} or b_{jt}, representing its statistical weight. No more than two metabolites were used in each classification ($0 < k \leq 2$). The discriminant function F_{ij} summarizes this comparison, being calculated according to the following expressions:

$$Z = \sum_{t=1}^{k} a_{it} x_t - \sum_{t=1}^{k} b_{jt} x_t \quad (4)$$

$$C = a_0 - b_0 \quad (5)$$

$$F_i - F_j = Z + C \quad (6)$$

When classifying an intracranial biopsy between the tumor classes i and j, a positive value of the Fisher function $F_i - F_j$ assigns the sample to the tumor class i, and a negative value assigns it to class j. The probability that the investigated sample belongs to tumor classes i or j (p_i or p_j, respectively) is given by the expressions: $p_i = 1/[1 + \exp(-F_{ij})]$ or $p_j = 1 - p_i$, respectively.

The correct classification percentages for every pair of classes were validated by using the leave-one-out method. Briefly, every sample from a certain pair of classes was left out at a time to build a discriminant function with the rest of the samples included in the pair. Every time, the excluded sample was classified by using the discriminant function calculated without it, and thus correct classification percentages could be ascertained for both classes (29).

Multilateral classifications were also investigated. For every biopsy, the probability of belonging to a particular class P_i ($i = 1$–7) can be calculated as the product of the probabilities obtained from all bilateral comparisons where the considered class is involved (p_{im}):

$$P_i = \prod_{m=1}^{n} p_{im}, \quad n = 7, \quad m = 1, 2, 3, \ldots, n, \quad m \neq i \quad (7)$$

Every sample is then assigned to the most probable class, defined as the one with the highest probability value P_i. This process makes it possible to calculate the percentage of correct classifications for each one of the seven tissue classes considered.

Materials

Phospholipid standards of the highest available quality were acquired from Sigma (St. Louis, MO, USA). Deuterated solvents (99.9% ^2H) were obtained from Apollo Scientific (Bradbury, Stockport, UK). The rest of the reagents were obtained from MERCK (Darmstad, Germany).

RESULTS

Phospholipid profiles from normal brain and brain tumors as detected by high-resolution ^{31}P-MRS

Figure 1 shows representative high-resolution ^{31}P-MRS spectra of phospholipid extracts from normal brain and also from the different brain tumors. Each resonance originates from the headgroup of a determined phospholipid, as indicated in the figure legend. Small deviations in the chemical shift of the individual phospholipids were observed within the different samples, derived from subtle changes in storage conditions, metal content, or the final chloroform/methanol proportion. In this respect, the most stable phospholipids were Alkyl-Acyl-PtdCho and PtdIns, whereas the ones more prone to variation and thus more sensitive to experimental conditions were the neutral zwitterions EtnPlas and PtdEtn. It should be

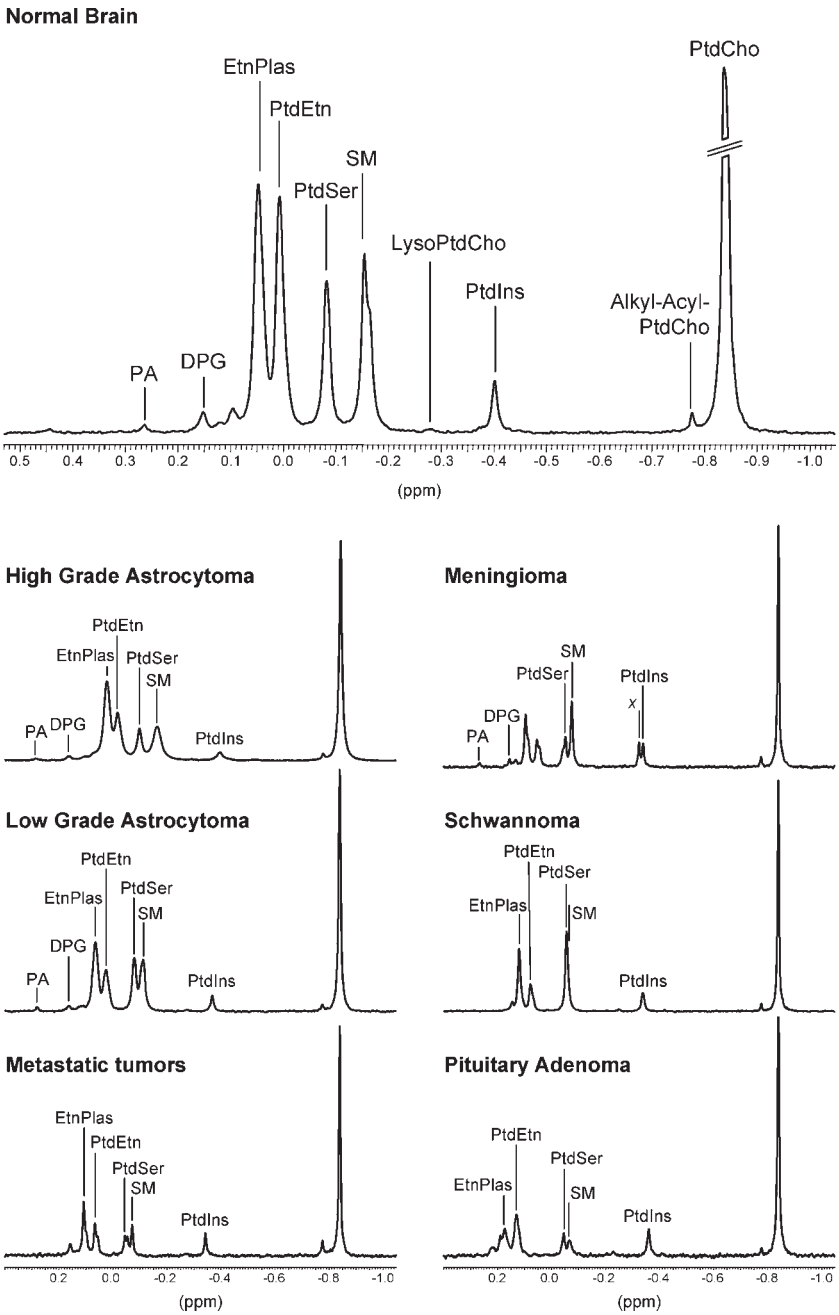

Figure 1. Representative ^{31}P-MRS spectra (202.4 MHz, 22°C) of chloroform/methanol phospholipid extracts from normal brain and the six tumor classes with three or more elements. Visual inspection reveals appreciable differences between the phospholipid profiles of normal brain and tumors, and also between the distinct tumor classes. PA: phosphatidic acid, 0.278 ± 0.037 ppm ($m \pm 2$ SD); DPG: diphosphatidylglycerol (cardiolipin), 0.172 ± 0.029 ppm; EtnPlas: ethanolamine plasmalogen, 0.111 ± 0.059 ppm; PtdEtn: phosphatidylethanolamine (cephalin), 0.069 ± 0.058 ppm; PtdSer: phosphatidylserine, -0.058 ± 0.029 ppm; SM: sphingomyelin, -0.087 ± 0.035 ppm; LysoPtdCho: lysophosphatidylcholine, -0.288 ± 0.043 ppm; *x*: unidentified phospholipid, $-0{,}353 \pm 0{,}035$ ppm; PtdIns: phosphatidylinositol, -0.362 ± 0.018 ppm; Alkyl-acyl-PtdCho: alkylacylphosphatidylcholine (choline plasmalogen), -0.777 ± 0.002 ppm; PtdCho: phosphatidylcholine (lecithin), -0.840 ppm (reference).

mentioned here that difficulties in the deconvolution of PtdSer and SM in some spectra of schwannomas may yield partially contaminated PtdSer variables in these tumors. In some spectra, some phospholipid resonances (EtnPlas, PtdEtn, and PtdSer) appeared to include two peaks, one forming a small shoulder on the other. Probably, the natural phospholipid resonance may include contributions from mixtures of different phospholipid entities, all of them having the same head group but different side chains, thus causing small shifts in the observed resonance. The possibility of a different phospholipid contributing to the superimposed resonances cannot be, however, excluded. In all these cases, we deconvoluted the resonances into two lorentzians and assigned to the indicated phospholipid the most abundant one, avoiding the contaminant.

PtdCho was the dominant phospholipid in all the cases, with important contributions from PtdEtn, PtdSer, EtnPlas, and SM. However, the phospholipid pattern, as reflected in the relative contributions of the different phospholipids to the total phospholipid content, is clearly different in the various tissues investigated, indicating a considerable potential for differential diagnosis.

Differences in phospholipid profiles as shown by univariate statistical analysis

Table 1 summarizes the descriptive statistics of the observed phospholipids and phospholipid ratios for each tumor class and normal brain. PtdCho accounted for up to 40% of the lipids detected by ^{31}P-MRS. The lyso-form of PtdCho constituted at most 2% of the phospholipid profile, confirming an adequate extraction technique with minimal phospholipid hydrolysis. No other lyso-forms were detected. There was a prevalence of EtnPlas over PtdEtn, ethanolamine phospholipids representing almost 30% of the gross phospholipid content in all the cases.

Table 2 details the statistically significant differences in phospholipid molar percentages and ratios that were found in the univariate analysis. Briefly, normal brain extracts had a significantly higher molar percentage of PtdEtn and a higher PtdEtn/PtdCho ratio than neuroepithelial (high-grade astrocytomas) and non-neuroepithelial tumors (meningiomas and schwannomas). High-grade astrocytomas showed decreased values of PtdEtn and PtdSer than the normal brain. Low-grade astrocytomas had a phospholipid profile similar to that for the normal brain, with the important exception of a lower PtdEtn and a slightly higher PtdCho content. Non-neuroepithelial tumors showed a trend toward elevated PtdIns and PtdCho as compared to normal tissue extracts. Meningiomas had almost double the proportion of Alkyl-acyl-PtdCho and increased PtdIns contribution compared to normal brain. Pituitary adenomas had the highest molar percentage of PtdIns and PtdCho in all the tumor classes, except gliosarcoma. Pituitary adenomas also harbored the lowest PtdSer and SM. Schwannomas displayed an increased molar percentage of PtdCho and PtdSer as compared to normal brain or metastatic lesions, respectively. Metastatic tumors were characterized by significantly lower values of PtdSer than the normal brain, low-grade astrocytomas and schwannomas. Metastases also showed a higher DPG content than low-grade astrocytomas and meningiomas. The PtdCho content of these lesions was increased as compared to the healthy tissue. Breast cancer metastasis had an EtnPlas/PtdEtn ratio lower than 1, showing a decrease in EtnPlas instead of PtdEtn in contrast to other metastases. Neuroepithelial tumor classes with less than three elements generally presented a reduction of PtdEtn, especially in malignant ependymoma, with a prevailing plasmalogen form and increased EtnPlas/PtdEtn ratio. Choroid plexus papilloma did not follow the same trend, with an EtnPlas/PtdEtn ratio similar to healthy tissue, although being the tumor with the highest content of choline plasmalogen (5.9%).

Classification of biopsies using phospholipid profiles and step-wise linear discriminant analysis

Bilateral classifications

Fisher functions calculated for every pair of classes are listed in Table 3. Because of the reduced sample size, no more than two variables were used in each function. Note that variables which classified better the normal brain from non-metastatic tumors are PtdEtn and those ratios include PtdEtn in the numerator. As it was found by univariate analysis, a higher content of PtdIns was helpful to classify non-neuroepithelial tumors and a low PtdSer content favored the decision for metastatic tumors. Ethanolamine phospholipids and PtdSer appear to be important for the differentiation between low- and high-grade astrocytomas.

Table 4 presents the percentage of successful classifications for every pair of tumor classes, as calculated from the Fisher functions described above (*cf* Table 3). Almost half of the classifications performed showed an accuracy of 100%. The classes with better classification scores were: normal brain, meningiomas, high-grade astrocytomas, and metastatic tumors, with 71–100% of correct assignments. Low-grade astrocytomas and schwannomas provided the less favorable results.

Multilateral classification

Table 5 contains the results of multilateral classification. In this analysis, each sample was classified into one of the seven possible classes in the dataset. First, the molar percentages of each phospholipid determined by ^{31}P-NMR were substituted in the appropriate Fisher functions (Table 3), yielding for each one of the biopsies the probability of belonging to each one of the two classes compared. The probability that a given biopsy belongs to each one of the seven considered classes could be then calculated as the product of the probabilities obtained in all bilateral comparisons involving the investigated class. The most probable class was the one with the highest probability value. Using this approach, it was possible to classify correctly up to 68% of the biopsy extracts between the seven tissue classes considered. The specificity was higher than the sensitivity in all the classes, which means that the probability of assigning a phospholipidic extract to an incorrect class was much smaller than the probability of assigning it to the correct class. When considering the percentages of sensitivity and specificity, normal brain samples could be perfectly differentiated from all other tumor classes; meningiomas, metastases, and high-grade astrocytomas also gave good classification results, in a decreasing order (Table 5). Eleven of the samples were misclassified, as listed in the last column of Table 5. If the samples were assigned at random, the expected sensitivity for each class would be 14.3%. Our approach provides a significant improvement over this value.

Table 1. Relative phospholipid contributions and phospholipid ratios in normal brain, neuroepithelial, non-neuroepithelial, and metastatic tumors.

Histological Class	*n*	PA	DPG	EtnPlas	PtdEtn	PtdSer	SM	Lyso PtdCho	PtdIns	Alkyl-Acyl PtdCho	PtdCho	PtdEtn/ PtdCho	TEtn/ PtdCho	PtdSer/ PtdCho	PtdIns/ PtdCho	PtdEtn/ PtdSer	TEtn/ PtdSer	PtdIns/ PtdEtn	PtdIns/ TEtn	PtdIns/ PtdSer
Normal brain	3	0.9 (0.4)[a]	0.6 (0.3)	19.9 (2.4)	16.6 (0.8)	13.6 (0.7)	7.2 (1.2)	0.4 (0.1)	3.0 (0.1)	0.7 (0.2)	35.1 (0.8)	0.47 (0.02)[b]	1.04 (0.08)	0.39 (0.01)	0.08 (0.01)	1.23 (0.04)	2.72 (0.28)	0.18 (0.01)	0.08 (0.00)	0.22 (0.02)
Neuroepithelial tumors																				
High-grade astrocytomas	7	0.4 (0.2)	1.0 (0.2)	17.5 (1.9)	10.5 (1.3)	10.1 (1.3)	10.2 (1.2)	1.8 (0.8)	3.7 (0.4)	2.2 (0.7)	41.3 (2.5)	0.26 (0.04)	0.70 (0.08)	0.26 (0.05)	0.09 (0.01)	1.20 (0.23)	3.10 (0.48)	0.40 (0.08)	0.14 (0.03)	0.39 (0.04)
Low-grade astrocytomas[c]	4	0.8	0.8 (0.1)	20.6 (1.6)	11.1 (3.0)	14.2 (2.1)	8.5 (2.2)	0.4	4.5 (1.8)	1.4 (0.3)	38.2 (2.4)	0.28 (0.07)	0.84 (0.05)	0.38 (0.07)	0.12 (0.05)	0.87 (0.25)	2.42 (0.43)	0.89 (0.68)	0.15 (0.07)	0.30 (0.08)
Oligodendrogliomas	2	0.6 (0.1)	0.3 (0.2)	20.9 (4.6)	11.3 (0.7)	13.9 (0.8)	11.4 (0.2)	0.7	5.4 (2.1)	0.5 (0.2)	35.0 (2.6)	0.32 (0.00)	0.94 (0.18)	0.40 (0.05)	0.15 (0.05)	0.82 (0.10)	2.31 (0.15)	0.47 (0.16)	0.18 (0.09)	0.40 (0.18)
Ependymoma	1	—	0.8	21.4	8.0	12.7	12.4	3.4	3.9	1.1	35.5	0.22	0.83	0.36	0.11	0.63	2.32	0.48	0.13	0.31
Central neurocytoma	1	0.7	3.0	16.7	11.3	8.4	13.6	1.2	4.2	0.7	37.5	0.30	0.75	0.22	0.11	1.35	3.34	0.37	0.15	0.50
Choroid plexus papilloma	1	—	1.3	10.5	8.5	10.5	16.4	0.5	5.1	5.9	34.4	0.25	0.55	0.31	0.15	0.81	1.81	0.60	0.27	0.49
Gliosarcoma	1	—	—	17.6	7.7	12.2	6.7	4.1	1.0	3.0	47.8	0.16	0.53	0.25	0.02	0.63	2.08	0.13	0.04	0.08
Subtotal	17	0.6 (0.1)	1.0 (0.2)	18.4 (1.1)	10.4 (0.8)	11.7 (0.8)	10.4 (0.8)	1.8 (0.5)	4.1 (0.5)	1.9 (0.4)	39.2 (1.4)	0.27 (0.02)	0.75 (0.05)	0.31 (0.03)	0.11 (0.02)	1.00 (0.12)	2.68 (0.24)	0.52 (0.16)	0.15 (0.02)	0.36 (0.04)
Non-neuroepithelial tumors																				
Meningiomas	9	0.6 (0.1)	0.8 (0.1)	15.7 (2.0)	10.0 (1.2)	12.5 (1.7)	11.5 (1.2)	1.8 (0.8)	4.9 (0.4)	1.3 (0.1)	41.2 (1.8)	0.25 (0.03)	0.65 (0.07)	0.31 (0.04)	0.12 (0.01)	0.88 (0.14)	2.30 (0.31)	0.54 (0.06)	0.20 (0.03)	0.42 (0.04)
Schwannoma	3	—	0.5 (0.4)	18.6 (1.9)	7.1 (2.4)	14.3 (2.5)	11.4 (2.8)	0.6 (0.1)	4.5 (0.8)	1.7 (0.5)	41.4 (1.6)	0.18 (0.06)	0.62 (0.05)	0.35 (0.06)	0.11 (0.02)	0.58 (0.25)	1.92 (0.37)	0.85 (0.34)	0.17 (0.02)	0.33 (0.06)
Pituitary adenomas	4	0.7 (0.3)	1.0 (0.3)	15.6 (2.0)	13.4 (2.5)	7.7 (1.9)	6.4 (1.6)	2.1 (0.9)	8.0 (2.1)	1.2 (0.1)	44.5 (3.1)	0.31 (0.06)	0.67 (0.08)	0.18 (0.06)	0.18 (0.05)	2.01 (0.53)	4.28 (0.74)	0.62 (0.14)	0.27 (0.05)	1.27 (0.40)
Subtotal	16	0.6 (0.1)	0.8 (0.1)	16.2 (1.3)	10.3 (1.1)	11.6 (1.2)	10.2 (1.0)	1.6 (0.5)	5.6 (0.6)	1.4 (0.1)	42.0 (1.3)	0.25 (0.03)	0.65 (0.04)	0.28 (0.03)	0.13 (0.02)	1.11 (0.20)	2.72 (0.34)	0.62 (0.08)	0.21 (0.02)	0.62 (0.14)
Metastatic tumors																				
Breast	2	0.4 (0.1)	1.4 (0.2)	12.1 (5.9)	18.3 (1.2)	8.1 (1.7)	8.7 (2.5)	1.5 (1.1)	4.4 (2.4)	0.7 (0.1)	43.2 (7.9)	0.43 (0.05)	0.75 (0.24)	0.20 (0.08)	0.09 (0.04)	2.38 (0.64)	3.78 (0.20)	0.23 (0.12)	0.16 (0.10)	0.62 (0.42)
Lung	1	0.5	2.2	17.6	8.8	7.7	7.0	0.4	5.5	3.3	44.7	0.20	0.59	0.17	0.12	1.15	3.46	0.63	0.21	0.72
Melanoma	1	—	—	24.8	9.0	8.0	11.5	—	4.8	2.9	39.0	0.23	0.87	0.21	0.12	1.12	4.20	0.53	0.14	0.59
Subtotal	4	0.4 (0.1)	1.6 (0.3)	16.7 (3.9)	13.6 (2.8)	8.0 (0.7)	9.0 (1.4)	1.1 (0.7)	4.8 (1.0)	1.9 (0.7)	42.5 (3.5)	0.32 (0.07)	0.74 (0.11)	0.20 (0.03)	0.11 (0.02)	1.76 (0.44)	3.81 (0.17)	0.40 (0.11)	0.17 (0.04)	0.64 (0.18)
Total	40	0.6 (0.1)	1.0 (0.1)	17.5 (0.8)	11.1 (0.7)	11.4 (0.6)	10 (0.6)	1.5 (0.3)	4.7 (0.4)	1.6 (0.2)	40.4 (0.9)	0.28 (0.02)	0.73 (0.03)	0.29 (0.02)	0.12 (0.01)	1.13 (0.11)	2.81 (0.18)	0.52 (0.08)	0.17 (0.01)	0.48 (0.06)

[a]Values are expressed in molar percentages, as mean (standard error) of *n* biopsies.
[b]Ratios are expressed as mean (standard error).
[c]Phospholipid only identified in one biopsy.

Table 2. Comparisons of relative phospholipid content between pairs of tissue classes.[a]

	Normal brain	High grade astrocytomas	Low grade astrocytomas	Meningiomas	Schwannomas	Pituitary adenomas	Metastases
Normal brain ($n=3$)		PtdEtn (0.017)[b] PtdSer (0.047) PtdEtn/PtdCho (0.006) TEtn/PtdCho (0.041) PtdSer/PtdCho (0.034)		PtdEtn (0.012) PtdEtn/PtdCho (0.002) TEtn/PtdCho (0.011)	PtdEtn (0.021) PtdEtn/PtdCho (0.011) TEtn/PtdCho (0.011)	TEtn/PtdCho (0.023) PtdSer/PtdCho (0.027)	PtdSer (0.003) PtdSer/PtdCho (0.004)
High grade astrocytomas ($n=7$)	PtdIns/PtdSer (0.025)						
Low grade astrocytomas ($n=4$)					TEtn/PtdCho (0.037)		PtdSer (0.028)
Meningiomas ($n=9$)	Alkyl-Acyl-PtdCho (0.016) PtdIns (0.025) PtdIns/PtdEtn (<0.001) PtdIns/TEtn (0.047) PtdIns/PtdSer (0.022)					SM (0.031)	
Schwannomas ($n=3$)	PtdCho (0.026)						PtdSer (0.038)
Pituitary adenomas ($n=4$)	PtdIns/TEtn (0.031)	PtdIns (0.025) PtdIns/TEtn (0.036)		TEtn/PtdSer (0.012)			
Metastases ($n=4$)	TEtn/PtdSer (0.018)		DPG (0.045) TEtn/PtdSer (0.025)	DPG (0.012) PtdEtn/PtdSer (0.031) TEtn/PtdSer (0.010)	TEtn/PtdSer (0.004)		

[a]Comparisons are performed for the same phospholipid between two tissue classes. Only statistically significant results are shown. Significance *p*-values are indicated in parentheses to the right of each phospholipid, as calculated using the Student *t*-test. The statistically significant variables shown in each cell have a higher value for the class in the corresponding row and a lower value for the class in the corresponding column. For example, normal brain shows higher PtdSer content and higher PtdSer/PtdCho when compared to metastatic tumors.
[b]Variable (*p*-value).

Table 3. Fisher discriminant functions ($F_{ij} = F_i - F_j$) obtained for the binary classification of biopsy extracts between tissue classes with more than three elements.[a]

$F_1 - F_2 = 29.952$ PtdEtn/PtdCho $- 11.811$[b]
$F_1 - F_3 = 0.250$ PtdEtn $- 3.743$
$F_1 - F_4 = 33.529$ PtdEtn/PtdCho $- 13.165$
$F_1 - F_5 = 46.335$ PtdEtn/PtdCho $- 15.035$
$F_1 - F_6 = 16.222$ TEtn/PtdCho $- 14.144$
$F_1 - F_7 = 3.241$ PtdSer $- 35.172$
$F_2 - F_3 = -0.663$ PtdSer $- 1.320$ TEtn/PtdSer $+ 12.251$
$F_2 - F_4 = -0.885$ PtdIns $+ 3.587$
$F_2 - F_5 = -2.598$ PtdIns/PtdEtn $- 0.151$ PtdSer $+ 4.321$
$F_2 - F_6 = -4.065$ PtdIns/PtdSer $+ 3.941$
$F_2 - F_7 = -5.287$ PtdIns/PtdSer $+ 3.282$
$F_3 - F_4 = 7.137$ TEtn/PtdCho $- 8.744$ PtdIns/PtdSer $- 2.956$
$F_3 - F_5 = 22.004$ TEtn/PtdCho $- 15.792$
$F_3 - F = -2.957$ PtdIns/PtdSer $+ 2.331$
$F_3 - F_7 = -3.183$ TEtn/PtdSer $+ 9.908$
$F_4 - F_5 = -3.382$ PtdIns/PtdEtn $+ 3.449$
$F_4 - F_6 = -4.663$ PtdIns/PtdSer $+ 4.759$
$F_4 - F_7 = -2.350$ TEtn/PtdSer $+ 7.984$
$F_5 - F_6 = -1.594$ TEtn/PtdSer $+ 4.658$
$F_5 - F_7 = -7.975$ TEtn/PtdSer $+ 22.557$
$F_6 - F_7 = 10.528$ PtdIns/TEtn $- 2.304$

[a]Fisher discriminant functions for the binary comparison of classes *i* and *j* are expressed in the notation $F_i - F_j$ (F_{ij}). Subscripts *i* and *j* indicate the two tissue classes compared: class 1, normal brain; class 2, high grade astrocytomas; class 3, low grade astrocytomas; class 4, meningiomas; class 5, schwannomas; class 6, pituitary adenomas; class 7, metastatic tumors.
[b]A positive sign of a variable in a certain function $F_i - F_j$ (F_{ij}) indicates that the value of this variable is directly proportional to the probability of the sample belonging to class *i*, and inversely proportional to the probability of the sample of belonging to class *j*. E.g. in $F_1 - F_3$ (F_{13}), the higher the PtdEtn the more probable the sample is classified as normal brain.

DISCUSSION

Assessment of phospholipid profiles of brain tumors by MRS methods

Alterations in the phospholipid content have been reported to occur in many tumors, yet the identification of the specific relationships between changes in the phospholipid profile and the particular tumor type remains elusive (7). ^{1}H and ^{31}P-MRS provide novel diagnostic tools to comprehensively investigate the biochemical alterations that occur in intracranial tumors, particularly those involving phospholipid metabolism. However, progress in the characterization of phospholipid profiles of the different neoplasms has been limited by the insufficient sensitivity and resolution of *in vivo* clinical ^{1}H or ^{31}P-MRS. Limited *in vivo* resolution of the phospholipid profiles stems from the fact that most phospholipids are incorporated in cell membranes, and their resonances become broadened or even undetectable *in vivo* in these circumstances. Direct observation of the phospholipid profile by MRS requires the extraction of the tissue with organic solvents, such as chloroform/methanol. Phospholipid analysis by ^{31}P-MRS has remained limited, however, because of the lack of a reliable method to assess and compare quantitatively the different spectra. Simple visual assessment provides no reliable information, essentially precluding the quantitative discrimination of the pattern of phospholipid resonances that characterize a specific tumor. This may be significantly improved through the use of multivariate analysis procedures, a statistical approach that allows the unambiguous characterization of the profile defining a specific tumor type or grade. Linear discriminant analysis has been used previously for the discrimination of ^{1}H-MRS spectra of brain tumor extracts, with satisfactory scores, close to 100% in some favorable cases (3–5). The main objective of this pilot study was to investigate the diagnostic possibilities offered by discriminant multivariate methods when applied to the analysis of phospholipid profiles of intracranial tumors as derived from the ^{31}P-MRS analysis of chloroform/methanol extracts.

Table 4. Scores obtained in the classifications between all possible combinations between two tissue classes using the Fisher functions listed in Table 3.[a]

	Normal brain (%)	High grade astrocytomas (%)	Low grade astrocytomas (%)	Meningiomas (%)	Schwannomas (%)	Pituitary adenomas (%)	Metastatic tumors (%)
Normal brain		100	100	100	100	100	100
High grade astrocytomas	86		71	71	86	100	100
Low grade astrocytomas	75	75		50	100	100	75
Meningiomas	89	78	78		100	100	78
Schwannomas	100	67	67	0		100	100
Pituitary adenomas	75	75	75	75	75		75
Metastatic tumors	100	50	100	100	100	75	

[a]Only tissue classes containing more than three elements are considered. The score represents the percentage of correct classifications in which the algorithm and histological diagnosis agreed. Table should be read following the rows. Every row lists the percentage of the results obtained in the bilateral classifications (leave-one-out cross-validation method, see text for details) of the phospholipid profiles indicated in the left column with those of each one of the other six tissue classes. E.g., when classifying normal brain (class 1) and high grade astrocytoma (class 2) extracts by using the Fisher function F_{12} listed in Table 3, a 100% of correct assignments were obtained in normal brain extracts, and 86% in high grade astrocytoma extracts.

Table 5. Discriminant analysis: Multilateral classification.[a]

Histological class	*n*	True positives	False positives	Sensitivity[b] (%)	Specificity[c] (%)	Incorrect classifications
Normal brain	3	3	0	100	100	
Neuroepithelial tumors						
High grade astrocytomas	7	4	4	57	85	2 classified as meningioma[d] 1 classified as low grade astrocytoma[e]
Low grade astrocytomas	4	2	1	50	97	1 classified as high grade astrocytoma[e] 1 classified as schwannoma[d]
Non-neuroepithelial tumors						
Meningioma	9	8	4	89	84	1 classified as high grade astrocytoma[f]
Schwannoma	3	1	1	33	97	1 classified as meningioma 1 classified as high grade astrocytoma [f]
Pituitary adenoma	4	2	0	50	100	1 classified as metastatic tumor[g] 1 classified as high grade astrocytoma[f]
Metastatic tumors	4	3	1	75	97	1 classified as meningioma

[a]The classification was accomplished as indicated in 'Experimental' section. Briefly, the molar percentages determined from the ^{31}P-MRS spectrum were substituted in the Fisher functions of Table 3. The probability that the sample belongs to each of the seven classes considered can be calculated as the product of probabilities of all binary comparisons concerning each class. The sample is then classified in the class showing the highest probability.
[b]Sensitivity: percentage of correct classifications for any given class.
[c]Specificity: percentage of true negatives for any given class.
[d]Two high grade astrocytomas were classified as meningiomas and a sample of a low grade astrocytoma as a schwannoma, due to the abnormally high contents of PtdIns in those particular extracts (5.3 and 4.8%, respectively).
[e]A high content of PtdSer (14.2%) in an extract from a high grade astrocytoma led us to misclassify this sample as a low grade astrocytoma and, contrarily, a lower PtdSer (9.2%) favored a misclassification of one of the low grade astrocytomas as high grade.
[f]An extract from a meningioma and one from a pituitary adenoma were classified in the high grade astrocytoma class, mainly because of the decreased contents of PtdIns, which values were lower than the mean expressed by the corresponding classes (2.5 and 3.88%, respectively). Also, one schwannoma was misclassified as a high grade astrocytoma due to a low PtdIns/PtdEtn ratio (0.41).
[g]A low PtdIns/PtdEtn ratio (0.42) influenced the misdiagnosis of a biopsy of pituitary adenoma as a metastatic tumor.

Alterations in specific phospholipids in intracranial tumors

Phospholipid molecules are not merely structural elements of the cell membrane, playing a vital active role in cellular physiology by mediation of the key signal transduction pathways controlling cellular survival and proliferation (30–33). Figure 2 illustrates the metabolic routes of synthesis and degradation of the major phospholipids PtdCho, PtdEtn, PtdSer, and SM, providing a useful frame to discuss the results obtained in this study.

Phosphatidylcholine

PtdCho is the major phospholipid component of eukaryotic cells, consequently providing the most prominent resonance in the ^{31}P-MR spectra of phospholipid extracts. PtdCho is involved in the membrane structure, signal transduction mechanisms, and lipoprotein metabolism (34). In this study, we observed a consistent trend toward an increased PtdCho content in intracranial tumors, supporting the increased membrane demands involved in cellular proliferation. As an example, high-grade astrocytomas presented a higher PtdCho proportion ($41.3 \pm 2.5\%$) than low-grade astrocytomas ($38.2 \pm 2.4\%$, ns) and the latter, higher than the normal brain. A similar high PtdCho fraction was also dteremined for non-neuroepithelial tumors and metastases, but this difference became statistically significant in the group of schwannomas. Increases in PtdCho content in gliomas, metastasis, and meningiomas has also been reported in previous ^{31}P-MRS and chromatography studies (16,35–37). Primary gliomas have shown strong inter-individual differences in phospholipid distribution, but the fractional contribution of PtdCho in glioblastomas may be up to a 30% higher than in lower grade astrocytomas (38). The increase in PtdCho and the resulting decrease in the PtdEtn/PtdCho ratio were the dominant features in the Fisher equations allowing for the best discrimination within most of the tumor classes – high grade astrocytomas, meningiomas, schwannomas, and pituitary adenomas – as compared to normal brain tissue. ^{31}P and ^{1}H-MRS studies performed in tumors, either under *in vivo* or *in vitro* conditions, reported an activation of both the anabolic and catabolic pathways for PtdCho, suggesting an increased turnover of this phospholipid (4,7,39). This could be explained by a combined activation of the enzyme choline kinase, the initial enzyme of the anabolic pathway, and of phospholipase-C, a catabolic enzyme that removes the PCho moiety of PtdCho and generates vital second messengers as DAG (40). The increased PtdCho resonance observed in many of the histological classes of intracranial tumors suggests a net balance of these processes favoring PtdCho accumulation.

Phosphatidylethanolamine

Overall, we observed a marked depletion of membrane PtdEtn in intracranial tumors as compared to the healthy brain tissue. In particular, we found a significant decrease in high-grade astrocytomas, meningiomas, and schwannomas. Other tumor classes also showed a non-significant trend toward decreased PtdEtn, with the exception of breast metastasis, which presented the highest PtdEtn value. Discriminant analysis revealed that PtdEtn is an essential variable for the diagnosis of normal brain, as it was selected by most of the Fisher functions that differentiate

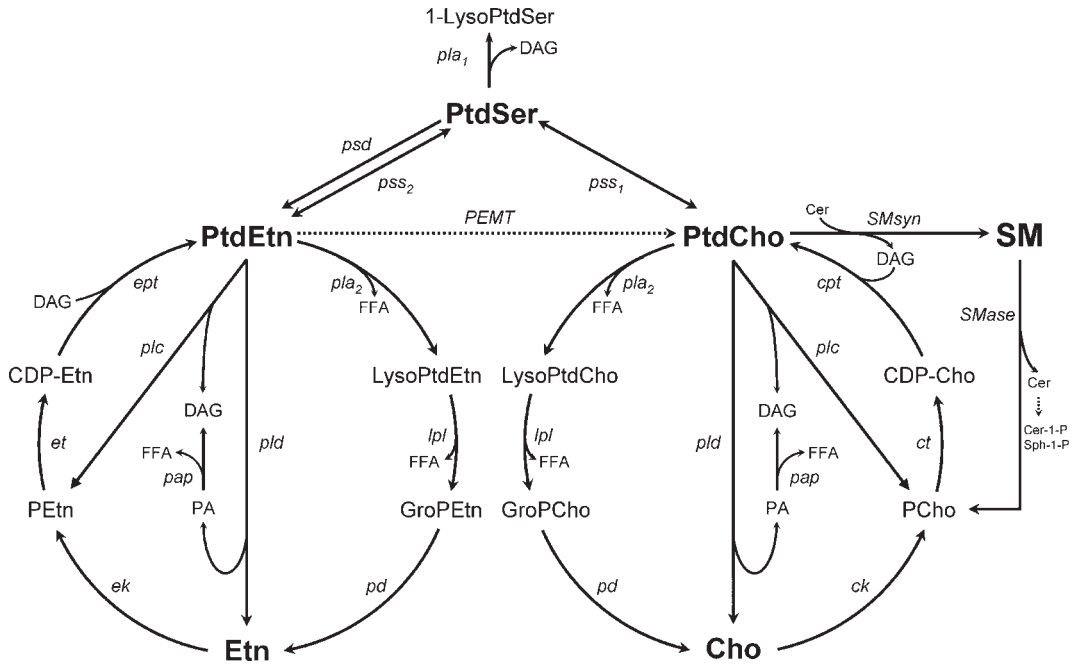

Figure 2. Metabolic pathways of phospholipid synthesis and degradation. Serine base exchange reactions with ethanolamine and choline by phosphatidylserine synthase I and II take place mainly in mitochondria-associated membranes, and there might be another isoform located in the endoplasmatic reticulum with serine-ethanolamine base exchange activity, as evidenced in CHO-K1 and murine liver cells (55). PtdEtn methylation occurs in mitochondria and, although a low phospholipid *N*-methyltransferase activity has been verified in the brain, it is significant only in the liver (56). Enzymes: ck, choline kinase; cpt, CDP-choline: 1,2-diacylglycerol cholinephosphotransferase; ct, CTP: phosphocholine cytidyltransferase; ek, ethanolamine kinase; ept, CDP-ethanolamine: 1,2-diacylglycerol ethanolaminephosphotransferase; et, CTP: phosphoethanolamine cytidyltransferase; lpl, lysophospholipase (phospholipase B); pap, phosphatidate phosphohydrolase; pd, phosphodiesterase; PEMT, phosphatidylethanolamine *N*-methyltransferase; pla_1, phospholipase A_1 (a pla_1 specific for PDS has been isolated in the human liver, testis, lung, and kidney, but its expression is low in brain); pla_2, phospholipase A_2; plc, phospholipase-C; pld, phospholipase D; psd, phosphatidylserine decarboxylase; pss_1, phosphatidylserine synthase I; pss_2, phosphatidylserine synthase II; SMase, sphingomyelinase; SMsyn, sphingomyelin synthase.

the healthy brain tissue from intracranial tumors. Our findings are supported by experimental and early chromatography studies, which reported decreases in PtdEtn content in gliomas (35,36,41,42), metastatic tumors (35), and in a Schwann cell line (NF1T) derived from a human neurofibroma (43). In the study by Merchant *et al*., the fractional molar contribution of PtdEtn was 22% lower in glioblastomas than in astrocytomas (16). As indicated in Fig. 2, the decrease in PtdEtn may be explained through an activation of the PtdEtn specific phospholipase-C (PLC) which cleaves this phospholipid into PEtn and DAG (44). Indeed, a PLC dependent degradation of PtdEtn in the brain has been described previously (33), and PtdEtn has been shown to be one of the most important sources of DAG in *ras*-transformed fibroblasts (45). In this sense, PtdEtn appears to represent a major source of DAG and intracellular mediators in cerebral neoplasms.

Other phospholipids

Interest in PtdSer metabolism has grown since it was included among the group of phospholipids that play a role in transmembrane signaling (30). Previous studies have reported a low PtdSer content in gliomas, meningiomas, undifferentiated neuroblastoma cells and brain metastasis of lung, breast, and stomach origin (21,31,35,41,42). In this study, we confirm the low PtdSer content in high grade astrocytomas, metastatic tumors and meningiomas, and we describe it in pituitary adenomas. The reduction in PtdSer may be the consequence of the increased activity of a specific phospholipase-A1 for PtdSer, the product of which, 2-lysophosphatidylserine, has been proposed to act as a second messenger (31). Additional causes for the depletion of PtdSer in tumors may be its decarboxylation into PtdEtn (30,31) or the exchange of serine for ethanolamine or choline by the PtdSer synthase enzyme (46).

PtdIns was found to be significantly increased in meningiomas, the PtdIns/PtdEtn ratio being significantly augmented in pituitary adenomas, which showed the highest molar percentage of this phospholipid in our dataset. In particular, PtdIns became important to discriminate non-neuroepithelial tumors in the corresponding Fisher functions. An increased PtdIns concentration in gliomas and meningiomas has been previously reported (37,41). In tumor cells, the accumulation of PtdIns and the need for second messengers in cell proliferation may be reciprocally related, as in the case of PtdCho (41). Signal transduction pathways in which PtdIns is involved, such as the PI3K–Akt pathway and the PtdIns–PKC system, have recently demonstrated to be important in high grade gliomas, meningiomas, pituitary adenomas, and certain metastatic cancers (47–50).

SM is the only phospholipid in the cellular membrane that is not derived from glycerol. We have identified a slight, but not significant, increase of SM, and the SM/PtdCho ratio in tumors (mainly in high grade astrocytomas and meningiomas) as compared to normal brain, except for pituitary adenomas. Although other ^{31}P-MRS reports have found reduced levels of SM in high-grade glial tumors when compared to meningiomas (38) and to neural sheath tumors (16), chromatography studies support our results (41). In our study, pituitary adenomas were the only tumors that showed a reduced SM/PtdCho ratio,

suggesting an increased sphingomyelinase activity in these tumors. This enzyme cleaves PCho from SM yielding ceramide, a well-known mediator of apoptosis under several stress conditions (51). SM may participate in cell death and proliferation by regulating the cellular levels of pro-apoptotic sphingolipids and DAG, a mitogenic second messenger (see Fig. 2) (32,52).

Classification of intracranial tumors by multivariate discriminant analysis of their phospholipid profile

Few attempts to use *in vitro* ^{31}P-MRS for automatic classification of tumors are available in the literature. By using cluster analysis, Howells *et al.* reported a 62% of global success in the classification of *in vivo* ^{31}P-MRS spectra of tumors implanted in animals (53). In a more recent study, Nadal *et al.* analyzed double extracts of 10 meningiomas and 10 glioblastomas *in vitro* by ^{1}H-MRS and ^{31}P-MRS, and grouped the data with multiple correspondences and ascending hierarchical classification methods. Although significant differences were found in one-dimensional analysis, the method of ascending hierarchical classification was not able to significantly discriminate between the two tumoral types (54).

A discriminant analysis performed to classify the biopsies among the seven tissue types that are included in our study would need to include more variables than it is allowed by our sample size in order to explain the metabolic variability between the classes. Since the sample size of our tissue types was relatively small, we were forced to use a limited number of phospholipids and ratios in the analysis. Thus, a simple discriminant analysis involving all the tissue classes together would not be able to provide acceptable classification scores. An innovative procedure was implemented to overcome this problem, in which linear discriminant analysis is applied separately to every pair of classes, and a discriminant function is calculated for every distinct pair. Depending on the sample size of the classes compared, only one or two variables (phospholipid metabolites or ratios) can be used to build the discriminant functions. Because the tissue classes are compared on a pairwise basis, we used the Student's *t* test instead of ANOVA for the identification of the relevant variables that would best perform in the discriminant analyses. This process allowed the selection of different variables for every pair of tissue classes, making it possible to consider more metabolic parameters, and respecting the limited degrees of freedom imposed by our reduced number of observations. These functions would allow the classification of a given sample between two tissue classes (bilateral classification). However, as described in our earlier study (5), the final correct classification scores (multilateral classification: classification of the samples between all the seven possible tissue classes) can then be ascertained by calculating the product of probabilities that were obtained from the previous bilateral discriminant functions.

With this methodology, all the phospholipid extracts of a normal brain were correctly discriminated, reaching an overall 68% successful discrimination among the seven histological classes included in the discriminant analysis. This is significantly better than the 14.3% successful classifications predicted for a random assignment within seven tumor classes. Moreover, as no tumor sample was misclassified as normal brain, these results indicate that membrane phospholipids can reliably differentiate a healthy tissue from a tumor. We are aware that the limited number of observations in our database may limit the scope of the results obtained with this classification method. A bigger number of samples per group would probably allow us to improve the present classification scores.

Concluding remarks

Our study shows that ^{31}P-MRS analysis of organic extracts from biopsies of normal brain and intracranial tumors is a useful tool to investigate the profile of membrane phospholipids. Extracts obtained from intracranial tumors demonstrate a consistent reduction of PtdEtn and PtdSer, and an increase of PtdCho and PtdIns contents. Linear discriminant analysis, as implemented in the present study, has proven to be robust enough to completely differentiate the normal brain from tumors by using their phospholipid profiles. However, it could not reach a completely successful differentiation between all the tumoral classes investigated when bilateral and multilateral comparisons were performed. Larger sample sizes, multinuclear investigations and the complement of additional techniques as genomic or proteomic approaches, may be further implemented to confirm the present findings, improving potentially the classification scores of the ^{31}P-MRS analysis of phospholipid profiles and allowing their transfer to clinical settings.

Acknowledgements

This study was supported in part by grants from the Spanish Ministry of Education and Science SAF 2004!03197 and NAN 2004-09125-C07-03, Grant S-BIO/0179/2006 from the Community of Madrid to SC. The authors are grateful to Dr María L. García-Martín and Dr María A. García-Espinosa for their useful technical and scientific advice. The authors also wish to acknowledge Mrs Cristina Benedicto for her invaluable help with the extraction of the biopsies and Dr Ana Poveda, from SiDi *Universidad Autónoma de Madrid*, for the ^{31}P-MRS of most of the extracts. Finally, the authors highly appreciate the help of Mr J. F. Solivera Gonzalez in the preparation of the final English version.

REFERENCES

1. Sjøbakk TE, Johansen R, Bathen TF, Sonnewald U, Juul R, Torp SH, Lundgren S, Gribbestad IS. Characterization of brain metastases using high-resolution magic angle spinning MRS. NMR Biomed. 2008; 21: 175–185.
2. Opstad KS, Ladroue C, Bell BA, Griffiths JR, Howe FA. Linear discriminant analysis of brain tumour (1)H MR spectra: a comparison of classification using whole spectra versus metabolite quantification. NMR Biomed. 2007; 20: 763–770.
3. Tate AR, Underwood J, Acosta DM, Julia-Sape M, Majos C, Moreno-Torres A, Howe FA, van der Graaf M, Lefournier V, Murphy MM, Loosemore A, Ladroue C, Wesseling P, Luc Bosson J, Cabanas ME, Simonetti AW, Gajewicz W, Calvar J, Capdevila A, Wilkins PR, Bell BA, Remy C, Heerschap A, Watson D, Griffiths JR, Arus C. Development of a decision support system for diagnosis and grading of brain tumours using in vivo magnetic resonance single voxel spectra. NMR Biomed. 2006; 19: 411–434.
4. Herminghaus S, Dierks T, Pilatus U, Moller-Hartmann W, Wittsack J, Marquardt G, Labisch C, Lanfermann H, Schlote W, Zanella FE. Determination of histopathological tumor grade in neuroepithelial brain tumors by using spectral pattern analysis of in vivo spectroscopic data. J. Neurosurg. 2003; 98: 74–81.
5. Roda JM, Pascual JM, Carceller F, Gonzalez-Llanos F, Perez-Higueras A, Solivera J, Barrios L, Cerdan S. Nonhistological diagnosis of human cerebral tumors by 1H magnetic resonance spectroscopy and amino acid analysis. Clin. Cancer Res. 2000; 6: 3983–3993.
6. Maxwell RJ, Martinez-Perez I, Cerdan S, Cabanas ME, Arus C, Moreno A, Capdevila A, Ferrer E, Bartomeus F, Aparicio A, Conesa G, Roda JM,

Carceller F, Pascual JM, Howells SL, Mazucco R, Griffiths JR. Pattern recognition analysis of ^{1}H NMR spectra from perchloric acid extracts of human brain tumor biopsies. Magn. Reson. Med. 1998; 39: 869–877.
7. Podo F. Tumour phospholipid metabolism. NMR Biomed. 1999; 12: 413–439.
8. Ruiz-Cabello J, Cohen JS. Phospholipid metabolites as indicators of cancer cell function. NMR Biomed. 1992; 5: 226–233.
9. Kaibara T, Tyson RL, Sutherland GR. Human cerebral neoplasms studied using MR spectroscopy: a review. Biochem. Cell Biol. 1998; 76: 477–486.
10. Griffiths JR, Cady E, Edwards RH, McCready VR, Wilkie DR, Wiltshaw E. ^{31}P-NMR studies of a human tumour in situ. Lancet 1983; 1: 1435–1436.
11. Evanochko WT, Sakai TT, Ng TC, Krishna NR, Kim HD, Zeidler RB, Ghanta VK, Brockman RW, Schiffer LM, Braunschweiger PG. NMR study of in vivo RIF-1 tumors. Analysis of perchloric acid extracts and identification of ^{1}H, ^{31}P and ^{13}C resonances. Biochim. Biophys. Acta. 1984; 805: 104–116.
12. Sabatier J, Gilard V, Malet-Martino M, Ranjeva JP, Terral C, Breil S, Delisle MB, Manelfe C, Tremoulet M, Berry I. Characterization of choline compounds with in vitro 1H magnetic resonance spectroscopy for the discrimination of primary brain tumors. Invest Radiol. 1999; 34: 230–235.
13. Negendank W. Studies of human tumors by MRS: a review. NMR Biomed. 1992; 5: 303–324.
14. Certaines JD, Larsen VA, Podo F, Carpinelli G, Briot O, Henriksen O. In vivo 31P MRS of experimental tumours. NMR Biomed. 1993; 6: 345–365.
15. Tugnoli V, Tosi MR, Tinti A, Trinchero A, Bottura G, Fini G. Characterization of lipids from human brain tissues by multinuclear magnetic resonance spectroscopy. Biopolymers. 2001; 62: 297–306.
16. Merchant TE, van der Ven LT, Minsky BD, Diamantis PM, Delapaz R, Galicich J, Glonek T. ^{31}P NMR phospholipid characterization of intracranial tumors. Brain Res. 1994; 649: 1–6.
17. Seijo L, Merchant TE, van der Ven LT, Minsky BD, Glonek T. Meningioma phospholipid profiles measured by ^{31}P nuclear magnetic resonance spectroscopy. Lipids 1994; 29: 359–364.
18. Kleihues P, Louis DN, Scheithauer BW, Rorke LB, Reifenberger G, Burger PC, Cavenee WK. The WHO classification of tumors of the nervous system. J. Neuropathol. Exp. Neurol. 2002; 61: 215–225.
19. Folch J, Lees M, Sloane Stanley GH. A simple method for the isolation and purification of total lipides from animal tissues. J. Biol. Chem. 1957; 226: 497–509.
20. Meneses P, Glonek T. High resolution ^{31}P NMR of extracted phospholipids. J. Lipid. Res. 1988; 29: 679–689.
21. Merchant TE, Kasimos JN, Vroom T, de Bree E, Iwata JL, de Graaf PW, Glonek T. Malignant breast tumor phospholipid profiles using (31)P magnetic resonance. Cancer Lett. 2002; 176: 159–167.
22. Branca M, Culeddu N, Fruianu M, Serra MV. ^{31}P nuclear magnetic resonance analysis of phospholipids in a ternary homogeneous system. Anal. Biochem. 1995; 232: 1–6.
23. Friebolin H. The nuclear overhauser effect. In *Basic one- and Two-dimensional NMR Spectroscopy*. Wiley-VCH: Weinheim (Federal Republic of Germany), 1998; 287–300.
24. Klunk WE, Xu CJ, Panchalingam K, McClure RJ, Pettegrew JW. Analysis of magnetic resonance spectra by mole percent: comparison to absolute units. Neurobiol. Aging 1994; 15: 133–140.
25. Metz KR, Dunphy LK. Absolute quantitation of tissue phospholipids using ^{31}P NMR spectroscopy. J. Lipid Res. 1996; 37: 2251–2265.
26. Pascual JM, Carceller F, Cerdán S, Roda JM. Diagnóstico diferencial de tumores cerebrales "in vitro" por espectroscopía de resonancia magnética de protón. Método de los cocientes espectrales. Neurocirugia (Astur) 1998; 9: 4–10.
27. Afifi AA, Clarck VA, May S. Discriminant analysis. In *Computer-aided Multivariate Analysis*. Chapman & Hall/CRC: New York, 2004; 249–276.
28. Pascual JM, Solivera J, Prieto R, Barrios L, Lopez-Larrubia P, Cerdan S, Roda JM. Time course of early metabolic changes following diffuse traumatic brain injury in rats as detected by (1)H NMR spectroscopy. J. Neurotrauma 2007; 24: 944–959.
29. Huberty CJ, Olejnik S. Hit rate estimation. In *Applied MANOVA and Discriminant Analysis*. John Wiley & Sons, Inc.: Hoboken, NJ, 2006; 295–314.
30. Vance JE, Steenbergen R. Metabolism and functions of phosphatidylserine. Prog. Lipid Res. 2005; 44: 207–234.
31. Mozzi R, Buratta S, Goracci G. Metabolism and functions of phosphatidylserine in mammalian brain. Neurochem. Res. 2003; 28: 195–214.
32. Kolesnick R. The therapeutic potential of modulating the ceramide/sphingomyelin pathway. J. Clin. Invest. 2002; 110: 3–8.
33. Strosznajder J. Regulation of phosphatidylethanolamine degradation by enzyme(s) of subcellular fractions from cerebral cortex. Neurochem. Res. 1997; 22: 1199–1204.
34. Vance DE, Vance JE (eds). *Biochemistry of Lipids, Lipoproteins and Membranes*. Elsevier: New York, 2008.
35. Hattori T, Andoh T, Sakai N, Yamada H, Kameyama Y, Ohki K, Nozawa Y. Membrane phospholipid composition and membrane fluidity of human brain tumour: a spin label study. Neurol. Res. 1987; 9: 38–43.
36. Kokoglu E, Guner G, Guner A. Human brain tumor phosphoglycerides. Cancer Lett. 1984; 21: 325–328.
37. Riboni L, Ghidoni R, Sonnino S, Omodeo-Sale F, Gaini SM, Berra B. Phospholipid content and composition of human meningiomas. Neurochem. Pathol. 1984; 2: 171–188.
38. Lehnhardt FG, Rohn G, Ernestus RI, Grune M, Hoehn M. 1H- and (31)P-MR spectroscopy of primary and recurrent human brain tumors in vitro: malignancy-characteristic profiles of water soluble and lipophilic spectral components. NMR Biomed. 2001; 14: 307–317.
39. Ackerstaff E, Glunde K, Bhujwalla ZM. Choline phospholipid metabolism: a target in cancer cells? J. Cell. Biochem. 2003; 90: 525–533.
40. Glunde K, Jie C, Bhujwalla ZM. Molecular causes of the aberrant choline phospholipid metabolism in breast cancer. Cancer Res. 2004; 64: 4270–4276.
41. Ledwozyw A, Lutnicki K. Phospholipids and fatty acids in human brain tumors. Acta Physiol. Hung. 1992; 79: 381–387.
42. Martin DD, Robbins ME, Spector AA, Wen BC, Hussey DH. The fatty acid composition of human gliomas differs from that found in nonmalignant brain tissue. Lipids 1996; 31: 1283–1288.
43. Calderon RO, DeVries GH. Lipid composition and phospholipid asymmetry of membranes from a Schwann cell line. J. Neurosci. Res. 1997; 49: 372–380.
44. Gillies RJ, Morse DL. In vivo magnetic resonance spectroscopy in cancer. Annu. Rev. Biomed. Eng. 2005; 7: 287–326.
45. Momchilova A, Markovska T. Phosphatidylethanolamine and phosphatidylcholine are sources of diacylglycerol in ras-transformed NIH 3T3 fibroblasts. Int. J. Biochem. Cell Biol. 1999; 31: 311–318.
46. Wojcik M, Dygas A, Bobeszko M, Czajkowski R, Baranska J. Effect of ethanol on ATP-induced phospholipases C and D and serine base exchange in glioma C6 cells. Neurochem. Int. 2000; 36: 127–136.
47. Theodoropoulou M, Zhang J, Laupheimer S, Paez-Pereda M, Erneux C, Florio T, Pagotto U, Stalla GK. Octreotide, a somatostatin analogue, mediates its antiproliferative action in pituitary tumor cells by altering phosphatidylinositol 3-kinase signaling and inducing Zac1 expression. Cancer Res. 2006; 66: 1576–1582.
48. Mawrin C, Sasse T, Kirches E, Kropf S, Schneider T, Grimm C, Pambor C, Vorwerk CK, Firsching R, Lendeckel U, Dietzmann K. Different activation of mitogen-activated protein kinase and Akt signaling is associated with aggressive phenotype of human meningiomas. Clin. Cancer Res. 2005; 11: 4074–4082.
49. Hanew K, Utsumi A, Tanaka A, Ikeda H, Yokogoshi Y. Secretory mechanisms of growth hormone (GH)-releasing peptide-, GH-releasing hormone-, and thyrotropin-releasing hormone-induced GH release in patients with acromegaly. J. Clin. Endocrinol. Metab. 1998; 83: 3578–3583.
50. Bellacosa A, Kumar CC, Di Cristofano A, Testa JR. Activation of AKT kinases in cancer: implications for therapeutic targeting. Adv. Cancer Res. 2005; 94: 29–86.
51. Mathias S, Pena LA, Kolesnick RN. Signal transduction of stress via ceramide. Biochem. J. 1998; 335(Pt 3): 465–480.
52. Tafesse FG, Ternes P, Holthuis JC. The multigenic sphingomyelin synthase family. J. Biol. Chem. 2006; 281: 29421–29425.
53. Howells SL, Maxwell RJ, Howe FA, Peet AC, Stubbs M, Rodrigues LM, Robinson SP, Baluch S, Griffiths JR. Pattern recognition of ^{31}P magnetic resonance spectroscopy tumour spectra obtained in vivo. NMR Biomed. 1993; 6: 237–241.
54. Nadal L, Leray G, Desbarats C, Darcel F, Bansard JY, Bondon A, de Certaines JD. Proton and phosphorus nuclear magnetic resonance spectroscopy of human brain tumor extracts with automatic data classification: a preliminary study. Cell Mol. Biol. (Noisy-le-grand) 1997; 43: 659–673.
55. Stone SJ, Vance JE. Phosphatidylserine synthase-1 and -2 are localized to mitochondria-associated membranes. J. Biol. Chem. 2000; 275: 34534–34540.
56. Li Z, Vance DE. Phosphatidylcholine and choline homeostasis. J. Lipid Res. 2008; 49: 1187–1194.